Research Square

Preprints are preliminary reports that have not undergone peer review.
They should not be considered conclusive, used to inform clinical practice,
or referenced by the media as validated information.

Autophagy and intratumoral bacteria abundance influencing the prognosis of patients with pancreatic carcinoma

Franco Fortunato

Franco.Fortunato@uni-heidelberg.de

University Clinic Heidelberg https://orcid.org/0000-0002-6711-5828

Yifan Zhang

University Clinic Heidelberg

Toohina Gobin

University Clinic Heidelberg

Bingwen Miao

University Clinic Heidelberg

Zhenhua Huang

University Clinic Heidelberg

Roma Kurilov

German Cancer Research Center

Haitao Sun

University Clinic Heidelberg

Christine Tjaden

Technical University Munich

Ulrike Heger

University Clinic Heidelberg

Thilo Hackert

https://orcid.org/0000-0002-7012-1196

Ulf Hinz

University Hospital Heidelberg

Michael Schäfer

University of Heidelberg

Frank Bergmann

Institute of Pathology, University Hospital Heidelberg, Heidelberg

Christoph Springfeld

University Clinic Heidelberg

Sadaf Mughal

The German Cancer Research Center (DKFZ)

Benedikt Brors

Deutsches Krebsforschungszentrum https://orcid.org/0000-0001-5940-3101

Patrick Schaal

University Clinic Heidelberg

Bachar Cheaib

University Clinic Heidelberg

Danilo Licastro

AREA Science Park

Valerio Iebba

University of Trieste https://orcid.org/0000-0002-0716-306X

Article

Keywords:

Posted Date: April 27th, 2026

DOI: https://doi.org/10.21203/rs.3.rs-9358319/v1

License: This work is licensed under a Creative Commons Attribution 4.0 International License.
Read Full License

Additional Declarations: (Not answered)

Abstract

The biological and clinical significance of the intratumoral microbiota in pancreatic ductal adenocarcinoma (PDAC) remains poorly defined. Using oncogenic Kras-driven mouse models of pancreatic tumorigenesis and human pancreatic tissue from patients with non-metastatic PDAC treated with neoadjuvant (n = 62) or adjuvant therapy (n = 101), along with samples from intraductal papillary mucinous neoplasms (IPMN, n = 24), chronic pancreatitis (CP, n = 33), and healthy donors (n = 9), we determined tissue lipopolysaccharide (LPS), 16S rRNA sequencing, high-resolution quantitative multiplex immunofluorescence of autophagy markers (LAMP2, LC3B) and LPS, 16S rRNA fluorescence in situ hybridization (FISH) staining, and TLR4 signaling. In KrasCre mice, we identified significant bacterial accumulation in the pancreas, indicated by elevated LPS, increased FISH signals, enhanced TLR4 signaling, and activation of autophagy. Administration of exogenous LPS further amplified autophagy and TLR4 signaling, supporting a mechanistic link between microbial sensing and autophagy. In human tissue, both adjuvant and neoadjuvant PDAC samples showed significantly increased bacterial α- and β-diversity compared to controls, with similar enrichment in CP but not in IPMN, but with differed diversity patterns across the disease. Increased LPS levels along with elevated autophagy markers and abundant FISH-positive bacteria confirmed intratumoral colonization. Across four independent transcriptomic datasets PDAC samples showed elevated expression of bacterial-associated pathways (including TLR4) and autophagy-related genes. Clinically, higher autophagic activity of LAMP2_LC3B and increased densities of FISH-positive cells were independently associated with prolonged survival in both adjuvant and neoadjuvant or combined PDAC patients. Collectively, these findings link intratumoral microbial enrichment to enhanced autophagy/xenophagy and improved patient outcomes, suggesting that effective microbial handling within the tumor microenvironment favorably influences PDAC progression.

Introduction

Pancreatic adenocarcinoma (PDAC) is a highly aggressive cancer with an overall 5-year survival rate of approximately 13% and median survival remains low at approximately 4 months across all stages (1, 2). Despite advances in surgery and systemic therapy, PDAC remains the fourth leading cause of cancer-related death and is projected to become the second leading cause of cancer-associated mortality in developed countries within the next decade (1). Thus, there is an urgent need to identify novel biomarkers and therapeutic targets to improve patient outcomes. In recent years, there has been growing interest in the role of the microbiota, as dysbiosis has been implicated in cancer initiation and progression, including PDAC (3). The pancreas, once regarded as a sterile organ, is now recognized as a microbiologically active environment, capable of modulating disease pathogenesis and severity (4). Bacterial colonization of the pancreas is thought to occur via retrograde translocation from the duodenum through the pancreatic duct (5).

Microbes can penetrate pancreatic epithelial cells through well-established invasion pathways leading to intracellular localization (6). An evolutionarily conserved antibacterial autophagy pathway - xenophagy - eliminates intracellular pathogens by directing them to lysosomal degradation (7). Beyond maintaining

cellular homeostasis, xenophagy is a key host defense mechanism, limiting microbial persistence and infection (8). Accordingly, xenophagy represents a critical component of the innate immune response, while many pathogens have evolved sophisticated strategies to subvert or inhibit xenophagy, thereby promoting intracellular persistence and immune evasion (9-11) Chronic microbial persistence may therefore drive sustained inflammation and oncogenic signaling, increasing susceptibility to malignant transformation, as exemplified by *Helicobacter pylori* (12).

The intratumoral microbiota of PDAC is distinct from that of the healthy pancreas and varies across disease stage and metastatic progression (13-15). Recent experimental evidence demonstrates that microbial components such as LPS remodel the tumor microenvironment and synergizes with PD-L1 blockade to suppress tumor growth (16). Notably, increased microbial diversity has been associated with improved survival, suggesting that enrichment of intratumoral microbiota correlates with higher inflammatory responses and better survival. In addition, fecal microbiota transplantation experiments demonstrate that microbiota derived from long-term survivors can change the tumoral microbiota leading to reduced tumor growth, enhance immune cell infiltration and reduced PDAC tumorigenesis (17). Of note, emerging clinical studies suggest that probiotic supplementation may modestly extend survival in PDAC patients (18).

Autophagy plays a complex role in PDAC tumorigenesis. Genetic inhibition of autophagy leads to pancreatitis and pre-malignant lesions in mouse models, indicating a tumor-suppressive function early disease (19-21). Deletion of autophagy genes in hepatocytes promotes liver tumors, suggesting that autophagy loss promotes tumorigenesis (22). Beyond antimicrobial defense, xenophagy also shapes host immunity by modulating microbial antigen presentation and constraining excessive inflammatory cascades (23). However, although autophagy is elevated in PDAC, clinical trials targeting autophagy (e. g. Chloroquine) have shown limited efficacy (24-31). Importantly, the relationship between autophagy/xenophagy, the intratumoral microbiota, and clinical outcome in PDAC remains unclear.

In this study, we integrated 16S rRNA (16S ribosomal RNA) sequencing, FISH assay, and endotoxin (LPS) measurements to quantify intratumoral microbiota. To assess the link between bacterial burden and autophagy, we analyzed LAMP2_LC3B colocalization, as a surrogate marker of autophagy flux (32, 33). We show that autophagy correlates with the regulation of intratumoral microbial burden and this is associated with improved patients survival, revealing a functional microbiota-autophagy axis in PDAC.

Results

Accumulation of pancreatic bacteria in KrasCre mice.

We analyzed a Kras-driven PDAC mouse model (KrasCre) alongside Kras/B6 controls without LPS treatment. H&E staining revealed morphological alterations and tumor precursor lesions including acinar-to-ductal metaplasia (ADM) and pancreas-intraepithelial-neoplasia lesions (PanIN) (34) **(Fig. 1A)**. At older ages, KrasCre mice frequently develop the full spectrum of PanIN to invasive PDAC (35). Fluorescent in situ hybridization (FISH) detection of 16S rRNA **(Fig. 1B)**, demonstrated a marked

increase in bacterial abundance in KC pancreata (~6-fold) compared with control littermates **(Fig. 1C)**. PCR confirmed elevated bacterial load, with a 2.4-fold increase in rRNA in KC compared to control (14) **(Fig. 1D)**. Consistently, tissue endotoxin (LPS) enzymatic assay showed a 1.8-fold increase in KrasCre mice compared to controls **(Fig. 1E)**. These findings demonstrate that bacterial accumulation is an early feature of pancreatic tumorigenesis.

Elevated endotoxin activates pancreatic TLR-4 signaling.

To assess functional relevance, we quantified intrapancreatic LPS in KrasCre and Kras/B6 mice with or without LPS treatment **(Fig. 2A)**. Intraperitoneal (i. p.) LPS administration increased pancreatic LPS levels, with a stronger effect in KrasCre mice. Basal LPS levels without exogenous LPS treatment were ~9-fold higher detectable intra-pancreatic LPS level in KrasCre mice compared to Kras/B6 controls **(Fig. 2B/C)**. Moreover, the LPS-binding receptor Toll-like-receptor-4 (TLR4) expression was readily detectable and markedly elevated in KrasCre pancreata **(Fig. 2D/E)**. Notably, TLR4 expression increased ~42-fold in KrasCre mice under basal conditions compared with controls. These data indicate that microbial accumulation activates the LPS-TLR4 signalling axis in tumor-prone pancreas, even in the absence of exogenous stimulation.

Bacterial endotoxin enhances pancreatic autophagy

We assessed autophagy-related proteins in KrasCre and control mice +/- LPS treatment **(Supple. Fig. 1A)**. KrasCre mice exhibited increased expression of LAMP2, ATG5 and BECLIN1, alongside reduced p62 levels, consistent with enhanced autophagic flux. LPS treatment further amplified autophagy marker expression, while promoting LC3-I to LC3-II conversion (36). Basal microbial signals modestly activated autophagy, whereas LPS stimulation robustly enhanced this response **(Supple. Fig. 1B-F)**. This result collectively demonstrates that microbial products such as LPS and bacteria 16S rRNA representative for accumulation of intrapancreatic microbes drive autophagy activation in pancreatic tissue.

Microbiota accumulation in patients with chronic pancreatitis and intraductal papillary mucinous neoplasm.

We profiled intrapancreatic microbiota in chronic pancreatitis (CP) **(Table 1A)** and intraductal papillary mucinous neoplasm (IPMN) patients **(Table 1B)**, two conditions that increase the risk for developing PDAC. 16S sequencing revealed increased microbial alpha diversity in CP but not in IPMN compared to donor controls, as measured by Richness, Shannon, and Inverse Simpson indices **(Fig. 3A-C)**. IPMN exhibited lower diversity than CP, consistent with a prior study (37). However, at the genus level, the heat-map do not clearly visualized differences within the three groups **(Fig. 3D)**. In contrast, Beta diversity analysis showed distinct microbial communities in CP compared to controls and IPMN as determined by the ANOSIM and PERMANOVA indexes **(Fig. 3E)**. Endotoxin measurements revealed ~2-fold increase of gram-negative LPS (enzyme assay) in pancreatic tissue extracts from CP and IPMN patients compared to donor controls **(Fig. 3F)**. These finding indicate that microbial accumulation and composition shifts occur early during pancreatic disease progression.

Intratumoral microbiota are enriched in pancreatic adenocarcinoma.

We next analyzed intratumoral microbiota in tissue specimens from patients with adjuvant and neoadjuvant PDAC **(Table 1C)**. This approach revealed significantly elevated microbiota alpha diversity in adjuvant and neoadjuvant PDAC samples compared to donors, as indicated by the Richness, Shannon, and Inverse Simpson indices **(Fig. 4A-C)**. At the genus level, the heat map indicates an increased in the relative abundances of many bacteria in both adjuvant and neoadjuvant tissue compared to donor controls **(Fig. 4D)**. Beta diversity measured as the ANOSIM index showed a significantly different microbiota species in adjuvant PDAC compared to donor controls, while the PERMANOVA index identified differences between neoadjuvant PDAC compared to donor controls **(Fig. 4E)**. The accumulation of intratumoral bacteria were confirmed by an enzymatic gram-negative LPS assay using tissue extract. LPS increased 2.3-fold in adjuvant and 2.6-fold neoadjuvant PDAC tissues compared to donor pancreata **(Fig. 4F)**. We measured similar LPS concentrations of approximately 40 EU (endotoxin unit) per g tissue in murine *KrasCre* pancreata and human pancreata affected by pathologies (CP, IPMN, PDAC)**(Fig. 3F/4F)**. Additional microbial sensing pathways (TLR4, CD14, LBP, MyD88, MD2 mRNA expression) were almost all upregulated in PDAC transcriptomic datasets **(Supple. Fig. 2A)** All 5 mRNA species directly involved with the LPS signaling were all highly biologically meaningful (except LBP) elevated in a volcano blot **(Supple. Fig. 2B)** and also significantly increased in PDAC tissue representative in the GSE15471 database **(Supple. Fig. 2C)**. This finding suggests, that PDAC tissue show enriched microbiota with elevated TLR4 signaling.

Different microbiota species in PDAC, CP and IPMN

We further compared intra-pancreatic alpha diversity microbiota in tissue specimens from patients with CP, IPMN and combined both PDAC groups **(Table 1A-C)**. We detected significantly elevated microbiota alpha diversity in PDAC samples compared to CP and IPMN indicated by the Richness, Shannon, and Inverse Simpson indices **(Supple. Fig. 4A-C)**. At the genus level, the heat map indicates no visual differences within CP, IPMN and combined both PDAC groups **(Supple.Fig. 4D)** Beta diversity measured as the ANOSIM and PERMANOVA index showed a significantly different microbiota species in PDAC compared to CP and IPMN with more homogeneous microbiota species in PDAC and more diverse microbiota species in CP and IPMN **(Supple. Fig. 4E)**. Moreover, a volcano plot with abundance-scaled species enrichment revealed higher accumulation of *Microvirga* and *Porphyromonas* meanly in PDAC tissue and *Escherichia* and *Ligilactobacillus* meanly in CP/IPMN tissue, suggesting that CP and IPMN with high risk of developing PDAC show different intra-pancreatic bacterial species compared to PDAC **(Supple. Fig. 4F)**.

Bacterial enrichment correlates with improved survival in adjuvant and neoadjuvant pancreatic cancer patients.

We further determined independently marked increase bacterial signals of pancreatic LPS and FISH in adjuvant and neoadjuvant pancreatic cancer patients. IF signals for LPS substantial increase in adjuvant (20-folds) and neoadjuvant (40-fold) patients compared to donor controls **(Fig. 5A/B)**, which is in

accordance of the pancreatic enzymatic endotoxin/LPS concentration **(Fig. 4F)**. FISH 16S rRNA positive cells per mm^2 tissue increased by 4.5-fold in adjuvant PDAC and 6.2-fold neoadjuvant PDAC tissues compared to donor pancreata **(Fig. 5C/D)**. Furthermore, high levels of 16S rRNA FISH positive stained cells above median correlate with better survival in adjuvant PDAC with censored subjects included (median survival 33.08 months vs. 19.22)**(Fig. 5E)** and in neoadjuvant PDAC with censored subjects included (median survival 21.2 vs. 13.9 months) **(Fig. 5F)** or for the aggregate of both adjuvant and neoadjuvant PDAC with censored subjects included (median survival 29 vs. 18.3 months) **(Fig. 5G**). Of note, 16S FISH signals similarly increased 3.5- to 6-fold in mice and 4.4- to 6.4-fold in human PDAC **(Fig. 1C and Fig. 5D)**, suggesting similar enrichment of microbiota in mice and human. We identified 16S positive rRNA in PDAC tissues mainly within, or in close proximity to KRT19-positive pancreatic neoplastic cells, as well as in the stromal area **(Supple. Fig. 5A**). The 16S FISH show specific tissue staining with higher magnification and with a competition assay **(Supple. Fig. 5B/C**). 16S rRNA FISH also colocalized with a *Bacteroides* specific FISH probe with remarkable co-staining patterns and specificity validation by competition assays with cold probes **(Supple. Fig. 6A-C)**, with higher levels of either gram-positive or gram-negative bacteria and higher relative abundances of gram-negative *Bacteroides* and *Microvirga* in both adjuvant and neoadjuvant PDAC compared to normal pancreata **(Supple. Fig. 6D-G)**. These findings identify elevated intratumoral bacterial burden as a positive prognostic marker in PDAC patients.

Autophagy is associated with improved survival in adjuvant and neoadjuvant pancreatic cancer patients.

We further investigated autophagy as a potential mediator of microbiota-host interactions. Autophagy signaling has been shown to be elevated PDAC tissue (24, 25), we next determined the expression of LAMP2 and LC3B in PDAC tissue **(Fig. 6A)**. Autophagic activity, assessed by LAMP2_LC3B colocalization IF staining, was elevated in particular in neoadjuvant samples **(Fig. 6B-D)**. High autophagy levels with colocalization of LAMP2_LC3B strongly correlated with prolong survival across patients cohorts. In adjuvant PDAC patients, the median survival was 43.14 vs. 17.61 months and in neoadjuvant PDAC median survival was 20.96 vs. 12.81 months with both censored subjects included **(Fig. 6E/F)**. When analyzing LC3B alone or colocalization of LAMP2_LC3B in the aggregation of both adjuvant and neoadjuvant PDAC the median was survival was 25,13 vs. 17.61 months **(Fig. 6G. and Supple. Fig. 3C)**. Moreover, this survival association was further supported by transcriptomic analysis, where elevated LC3B mRNA showed better survival in the well-recognized Moffitt cohort with a survival above the median of 20.96 months vs. 12.81 months below the median with censored subjects included (38, 39) **(Fig. 6H)**. In addition, triple staining of LPS_LAMP2_LC3B, which is a sign of autophagosome with bacterial LPS (xenophagy) increased highly significantly by ~8-fold in adjuvant and by 11.7-fold in neoadjuvant PDAC patients compared to controls **(Supple. Fig. 3D)**. Moreover, triple positive dots of LPS_LAMP2_LC3B (xenophagosomes) increasing by ~3-fold in adjuvant and ~6-fold in neoadjuvant PDAC patients compared to controls **(Supple. Fig. 3E)**. LPS dots colocalized with LAMP2_LC3B dots in only 2 to 4 % of the cases, suggesting that only few LPS containing bacteria may be found in xenophagosomes. Interestingly, LAMP2 and LAMP2_LC3B are both significantly higher expressed in

neoadjuvant compared to adjuvant PDAC patients. We detected moderate elevated analyzed autophagy mRNA expression markers in four publicly available GSE transcriptomic datasets **(Supple. Fig. 7A-C)**. These finding suggest that microbial enrichment and autophagy are functionally linked and jointly associated with favorable outcomes.

Discussion

In this study, we demonstrate that intratumoral bacterial accumulation is a consistent feature of pancreatic ductal adenocarcinoma (PDAC) using multiple orthogonal approaches, including 16S sequencing of extracted DNA from cryo-conserved tissue, 16S rRNA fluorescence in situ hybridization (FISH) using FFPE tissue and two different independent bacterial endotoxin detection assays (enzymatic and antibody-based IF). The concordance across methods minimizes the likelihood of contamination and strengthens the robustness of our findings. Notably, high intratumoral bacterial load was associated with prolonged survival in both adjuvant and neoadjuvant PDAC patients, consistent with previous reports (14, 17). Those studies similarly link specific bacterial taxa to improve survival, supporting a functional role of microbiota in pancreatic tumor biology (17, 40). Emerging evidence further indicates that specific commensals can enhance anti-tumor immunity through activation of tumor-associated macrophages (TAMs), which could represent a novel clinical target to establish microbiota-targeted therapeutic paradigm for cancer intervention (41). For instance, *Limosilactobacillus* and *Blautia* has been show to correlate with better prognosis and both species have been associated with anti-tumor properties (42, 43). In our study we were unable to confirm these findings. However, the prognostic role of microbial diversity remains debated, likely due to the low biomass and technical variability inherent to pancreatic microbiome studies (14, 44-49).

Our results demonstrate a progressive microbial enrichment and reduce species diversity across disease stages indicates dynamic remodeling of pancreatic microbiota during tumor evolution. The marked expansion of the intratumoral microbial community in PDAC and intra-pancreatic in precursor disease such as CP and IPMN, likely reflecting translocation from the intestinal tract into a permissive oncogenic niche characterized by immune evasion and metabolic byproduct accumulation. This expansion was confirmed by elevated alpha-diversity indices, which were significantly higher in PDAC but also with different beta-diversity compared to CP, IPMN and healthy donor controls. The observed rising gradient of bacterial accumulation with different species from the precursor disease (CP and IPMN) to PDAC suggest that microbial colonization increases in tandem with tumor development. This is accompanied by activation of LPS-TLR4 signaling axis, highlighting functional engagement of microbial sensing pathways. The concordance across these diversity measures indicates that PDAC harbors a more abundant but more homogenous microbial community compared with non-malignant pancreatic states (15, 50).

We further investigated autophagy as a potential mediator of microbiota-host interactions. Increased autophagic activity strongly correlated with improved survival across the PDAC patient cohorts. In PDAC tissue, we observed elevated LPS colocalization with the autophagic markers LAMP2_LC3B, indicating

an abundance of xenophagosomes (autophagosomes containing bacterial LPS). These findings suggest a functional link between microbial enrichment and autophagy, both of which are jointly associated with favorable patient outcomes. Although autophagy has context-dependent roles in cancer, our results consistently show elevated autophagy markers and elevated 16S rRNA FISH in PDAC with a positive survival association. Methodological controls, including multiple negative controls and cross-validation across techniques, support the validity of our microbiome analysis.

The mechanisms by which the microbiota influences PDAC prognosis remain incompletely understood. We propose that autophagy facilitates the processing of intratumoral microbes, thereby modulating immune responses. Microbial signaling through TLR4 may enhance immunogenic pathways, thereby promoting anti-tumor immunity. Despite reports of immunosuppressive roles of autophagy, our results support a model in which, in the context of high microbial burden, autophagy contributes to a more immunological active anti-tumor microenvironment. Collectively, our findings define a bidirectional microbiota-autophagy axis that shapes PDAC biology and clinical outcome.

Methods

Patients Characteristics

The study was approved by the Ethics Committee of Heidelberg University for the use of human tissue samples (Approval No. S-141/2019 and S-083/2021), according to the Helsinki Declaration. This study included a retrospective patient cohort with FFPE tissue to determine LPS and autophagy by IF staining and cryo tissue to isolate tissue DNA (16S rRNA intra-pancreatic microbiota) and protein for tissue LPS (enzymatic assay). This study also included a prospective cohort, registered under DRKS00028995 at the German Clinical Trials Register. All tissues were collected and processed by the institutional tissue bank of the Department of Surgery Clinic at the Heidelberg University. Sample availability differed between experiments due to limited availability of matched FFPE and cryopreserved tissue. All patients provided written informed consent, and samples were pseudo-anonymised, according to the ethical guidelines. Patients were classified into five groups excluding PDAC with metastasis and PDAC with chemoradiation therapy: i) neoadjuvant PDAC Patients with locally advanced borderline unresectable tumor received treatment mFOLFIRINOX or gemcitabine-based therapy following surgical resection (n=62; ii) adjuvant chemo-naïve PDAC patients with resectable tumor at diagnosis (n=101; iii) patients diagnosed with intraductal papillary mucinous neoplasm (IPMN) (n=24); iv) patients diagnosed with chronic pancreatitis (CP) (n=33); v) healthy donor pancreata (n=9) **(Table 1A-C)**. All diagnoses were confirmed by histopathological evaluation. After surgical resection, tissues were either processed for formalin-fixed, paraffin-embedded (FFPE) tissues or snap frozen in liquid nitrogen. FFPE or cryo tissue were stained with Hematoxylin & Eosin (H&E) and were evaluated by a pancreas pathologist (FB) for staging and tumor content in the Department of Pathology as described recently (51). Clinical data are summarized in **Table 1A-C**.

Animals

Mice were maintained under standard semi pathogen-free conditions. All experiments were approved by the Institutional Animal Care and Use Committee at Heidelberg University in accordance with guidelines issued by the Federal Presiding Board for Animal Care, Karlsruhe, Germany (G-110/20, G-24/17). LSL-$Kras^{G12D}$ mice were crossed with Ptf1a/p48-Cre mice have a p48 promoter driven Cre recombinase to generate Kras-Crep48 (KrasCre) mice, were kindly provided by David Tuveson (34). All mice were maintained on a C57LB/6 background.

Animal experimental design

KrasCre and control Kras/B6 mice were used to assess intrapancreatic bacterial burden and autophagy signaling. Mice received intraperitoneal injections of LPS (2 mg/kg) or PBS twice weekly for 7 weeks starting at 25 weeks of age. Mice were euthanized at 31-weeks of age, and pancreas tissue was collected. Control Kras/B6 mice were treated with the same volume of PBS. Tissues were washed in sterile cold PBS, sterile cut into two pieces for either snap frozen in liquid nitrogen and kept at -80°C or immersed in 4% phosphate-buffered formaldehyde solution for preparing Formalin-fixed-paraffin-embedded (FFPE) tissue sections.

Genotyping

DNA was extracted using a standard tissue-to-PCR protocol (Thermo Fisher Scientific, Waltham, MA, USA). PCR amplification was performed using specific primers for the detection of Kras and p48-Cre, following by standard DNA electrophoresis, as described previously (20, 52, 53). The primers used in the PCR reaction are listed: Kras forward: 5'-CCTTTACAAGCGCACGCAGACTGTAGA-3', Kras reverse: 5'-AGCTAGCCACCATGGCTTGAGTAAGTCTGCA-3'; p48-cre forward: 5'-ACCGTCAGTACGTGAGATATCTT-3', p48-Cre reverse: 5'-ACCTGAAGATGT-TCGCGATTATCT-3'.

Endotoxin (LPS) assay

Frozen pancreatic tissue was homogenized and endotoxin level were quantified using a chromogenic endotoxin quant kit (Thermo Fisher Scientific) in microplate format according to the manufacturer's instructions and as described previously (20). For our samples, we measured Endotoxin Units (EU) per g of extracted pancreatic protein, which describe the biological impact of the endotoxins.

Fluorescence in situ hybridization (FISH)

FISH assay was performed on human and mouse FFPE tissue sections using a universal 16S rRNA probe (Alexa/650-5'-GCTGCCTCCCGTAGGAGT-3') and a *Bacteroides*-specific probe (Bfra602 ATTO594-5´-GAGCCGCAAACTTTCACAA-3´), both FISH probes has been described previously (14, 54, 55). After standard pre-treatment and hybridization, whole tissue sections were captured and analyzed using a TissueFAXS Fluorescence Imaging System (Tissue-Gnostics), with a fluorescence microscope unit, either Observer. Z1 (Zeiss and a Lumencor Sola SE III LED light source) or TissueFAXS LS slide loader for high-throughput analysis system for fluorescence Imaging (Tissue-Gnostics) and analysis StrataQuest

software version 7.0 (TissueGnostics), as described for the immune-fluorescence microscope unit, as described recently (20, 51, 52).

Western blotting (WB)

Human and mouse pancreas tissues were prepared under standard condition and protein levels were analyzed by SDS-PAGE and immunoblotting. ImageJ software was adopted for semi-quantification of the target-protein by calculating target fragment intensity divided by the loading/housekeeping control GAPDH, as described (52). The antibodies used in this study are listed in **Supple. Table 1.**

Immunofluorescence (IF)

Immunofluorescence staining for total tissue expression of LPS, LAMP2 and LC3B and the colocalization was performed using 4-µm-thin FFPE tissue sections. After antibody testing the anti-LAMP2 and anti-LC3B were direct labeled by using the SiteClick Alexa Fluor 647 sDIBO Alkyne (C20029) for LC3B and SiteClick Alexa Fluor 555 sDIBO (C20028) for LAMP2 according to the instructions. The anti-LPS was used with a secondary anti-mouse-AF 488 antibody. After the labelling procedure, direct and indirect labeled antibodies were also tested for functionality **(Supple. Table 1)**. Images were acquired using a TissueFAXS Fluorescence Imaging System (Tissue-Gnostics), with a fluorescence microscope unit, either Observer. Z1 (Zeiss and a Lumencor Sola SE III LED light source) and TissueFAXS LS slide loader high-throughput systems for up to 120 slides. Captured images were analyzed, which calculated the intensity of the fluorescence signals in each single cell within the entire individual tissue sections, as described recently (51).

DNA Extraction

DNA was extracted from human pancreatic cryo tissue under sterile conditions using Qiagen QIAamp DNA Mini Kits under rigorously contamination control according to the instruction. The tissue pieces were homogenized with an electric Teflon homogenizer, sterilized for every tissue piece in order to avoid cross contamination and to disrupt the bacteria cell wall. Extensive negative controls were included to monitor contamination at extraction and PCR stages. To detect lab-introduced contaminants, we processed a total of 615 negative controls alongside our samples. This included 308 DNA extraction controls to monitor for contamination during the initial DNA isolation steps (EB, elution buffer n=154; nFW, nuclease-free water n=154), and 307 no-template controls (NTCs) to check for contamination during the PCR amplification (PCRmix, PCR reagents with no template n=154; PCRmix_w_nfW, PCR reagents with nuclease-free water n=153). To also address potential contamination from FFPE slides we ran an additional 153 paraffin-only controls that were collected from paraffin blocks, without any tissue. Bacterial species retrieved from blank samples underwent a computation for pooled threshold at 99th percentile of relative abundance distribution as shown recently by Nejman et al. (14), and results (PDF with graphs, Excel file with statistics and raw data, text with explanation of Excel file tabs, whole analysis log file) are provided here: https://github.com/valerioiebba/PDAC-_blank_threshold/tree/main/PDAC_intratumoral_UPD. R script, along with necessary files and

instructions to reproduce the output files for blank threshold are provided within the GitHub repository: https://github.com/valerioiebba/PDAC_blank-_threshold/tree/main. Only species in positive samples whose relative abundance was higher or equal to the 99th percentile of blanks were kept for further analysis.

Real-time PCR

Bacterial abundance was quantified by qPCR targeting 16S rRNA , as described recently (14). The relative quantification was expressed as 2^(-ΔCt) as described previously (52). The primers for real-time PCR reaction are listed in **Supple. Table 1**. We also estimated bacteria DNA content in the tissue by determining bacterial 16S rRNA with a standard curve, which was calculated with increasing amounts of E. coli bacterial DNA, spiked into 150 ng of human DNA qPCR amplifications were made according to MIQE 2.0 guidelines (56).

16S rRNA Gene Sequencing

Microbiota analysis was conducted as described recently (57, 58). Extracted tissue DNA from donor control, PDAC, IPMN and CP pancreata were used to 16S rRNA protocol (59, 60). DNA quality was verified via Nanodrop spectrophotometry (A260/280 ratios), while quantification used Qubit fluorometry to ensure sufficient yield for 16S rRNA amplification (targeting V3-V4 regions). The 16S rRNA metagenomic library was prepared per the Illumina protocol (San Diego, CA, USA), amplifying the V3–V4 regions with denaturing primers in limited-cycle PCR, followed by AMPure XP bead purification (Beckman Coulter, Brea, CA, USA) (61). Dual-indexed adapters (Nextera XT Index Kit) were attached in a second PCR, with additional bead clean-up. Library concentration was quantified via Qubit 2.0 fluorometry (Invitrogen, Carlsbad, CA, USA) and validated on a Bioanalyzer DNA 1000 chip (1:50 dilution). After calculating nM concentrations based on amplicon size, libraries were pooled equimolarly and sequenced on an Illumina NovaSeq 6000 (2×300 bp, 5% PhiX spike-in) (62). Negative controls were included by applying the exact same extraction without clinical samples. (see “DNA Extraction” paragraph for specifications). PCR products were ligated to the sequencing adapters and paired-end sequenced on an Illumina MiSeq system (250 cycles).

Data analysis

Raw fastq files were analyzed with DADA2 pipeline v.1.14 for quality check and filtering (sequencing errors, denoising, chimerae detection). Filtering parameters were as follows: truncLen = 0, minLen = 100, maxN = 0, maxEE = 2, truncQ = 11, trimLeft = 15. All the other parameters in the DADA2 pipeline for paired-end were left as default. Bioinformatic and statistical analyses on recognized ASV were performed with Python v.3.8.2. Each ASV sequence underwent a nucleotide Blast using the National Center for Biotechnology Information (NCBI) Blast software (ncbi-blast-2.3.0) and the latest NCBI 16S Microbial Database (https://ftp://ftp.ncbi.nlm.nih.gov/blast/db/). Microbial species which did not have a biological meaning (environmental, rumen, extra-mammals, food, etc.) were excluded from raw data. In addition, a strengthened prevalence cutoff of 20% was employed in order to enrobust the differential

analysis (DA) (63-65), thus resulting in 73 species that were considered for subsequent statistical analyses. Measurements of α diversity (within sample diversity) such as Richness and Shannon index, were calculated at species level using the SciKit-learn package v1.0.1, starting from raw reads counts. Data matrices were processed for beta-diversity and differential analysis (DA) following three seminal papers which benchmarked against “ground-truth” the compositional data analysis in high- and low-complexity microbiome datasets (47, 64, 66). Data matrices were normalized and standardized using Quantile-Transformer and StandardScaler methods from Sci-Kit learn package v1.0.1 (67), ruling out total sum-scaling (TSS) or centered log-ratio (CLR) data transformations in order to avoid paradoxical results, especially in low-biomass or low-complexity microbial ecosystems. Normalization using the output_distribution = ’normal’ option transforms each variable to a Gaussian-like shaped distribution, whilst the standardization results in each normalized variable having a mean of zero and variance of one (67). Exploratory ecological analysis of β-diversity (between sample diversity) was calculated using the Bray-Curtis measure of dissimilarity and represented in Principal Coordinate Analyses (PcoA), along with methods to compare groups of multivariate sample units (analysis of similarities - ANOSIM, permutational multivariate analysis of variance - PERMANOVA) to assess significance in data points clustering. ANOSIM and PERMANOVA were automatically calculated after 999 permutations, implemented with custom scripts (Python v3.8.2, Seaborn v0.11.2, SciKit- learn v1.0.1) (68). We implemented Partial Least Square Discriminant Analysis (PLS-DA) and the subsequent Variable Importance Plot (VIP) as a supervised analysis, wherein the VIP values (equal or higher than 1, default settings) are used to identify the most discriminant bacterial species among the cohorts. Mann-Whitney U test and Kruskal-Wallis test were employed to assess significance for pairwise or multiple comparisons, respectively, considering a P value <= 0.05 as significant. Clustermaps of microbial abundances were generated with Euclidean distance and Ward linkage algorithms by means of custom scripts (Python v3.8.2, Seaborn v0.11.2, SciKit- learn v1.0.1). Where clearly stated, all *P*-values were corrected for multiple hypothesis testing using a two-stage Benjamini-Hochberg FDR at 10% (69).

Statistical Analysis and GEO database (Control vs. tumor expression analysis in PDAC)

We downloaded from the GEO database (https://www.ncbi.nlm.nih.gov/geo/) 4 publicly available PDAC expression datasets containing tumor and control samples (GSE15471 (70), GSE56560 (71), GSE62165 (72) and GSE62452 (73), with 254 PDAC and 120 controls without survival data. We also included the Moffitt cohort (GSE71729) with 123 PDAC because of the available PDAC survival data (38). We applied the software GraphPad Prism 6 for the survival analysis, using Kaplan-Maier and Log-rank Mantel-Cox test. All expression data were presented as Box and whiskers (Min to Max. show all points or 10-90 percentile). Statistical significance analysis was applied for multiple groups analysis by Student’s t-Test, nonparametric Mann-Whitney test comparing two groups analysis or for multiple testing using Mann-Whitney test with Holm-Bonferroni correction. The option of “identify outliers” of each target was also performed with this software. Results with p value ≤ 0.05 were considered to be statistically significant.

Declarations

Data availability statement

Raw FASTQ data of 16S targeted sequencing are available at NCBI Sequence Reads Archive - BioProject ID: PRJNA1310990.

Acknowledgments

The authors appreciate the substantial support from members of the European Pancreas Center (EPZ) - Biobank and PancoBank as well as the section of surgical research in Heidelberg: Sonja Bauer, Markus Fischer, Ingrid Herr, Sascha Hinterkopf, Karin Ruf, Miriam Schenk, Kathrin Schneider, Xu Zhou, Jingyu An, Teresa Peccerella, Wolfgang Groß, Nathalia Giese and Peer Bork. We greatly appreciate the support of David Tuveson, Paul Saftig and Risa Karakida Kawaguchi for kindly providing the transgenic mice. We would also like to thank Felix Bestvater and Manuela Brom for the help with the IF slide scanning (Zeiss Axioscan) and John P. Neoptolemos and Teresa Peccerella for the help with the IF TissueFAXS LS slide loader for high-throughput analysis system. Clinical data support was kindly provided by Markus W. Büchler, John P. Neoptolemos, Peter Bailey, Sophia Schäfer, Beate Köper, Katrin Tröltzsch, Antje Brockschmidt, Matthias Lang, Kai Hu, Thomas Hank, Arianeb Mehrabi, Guido Kroemer, Martin Loos and Christoph Michalski.

Ethics Statement

This study was approved by the Ethics Committee of Heidelberg University Hospital (approval number: S-206/2007 and S-443/2015). All procedures were performed in accordance with the Declaration of Helsinki. Written informed consent was obtained from all patients. Animal experiments were approved by the Regional Council of Karlsruhe (approval number: G-199/18).

Funding Statement

This work was supported by the Heidelberger Stiftung Chirurgie (F.F.) and the German Ministry for Education and Research (Bundesministerium für Bildung und Forschung, BMBF) grants 01GS08114 and 01ZX1305C (T.H.). The research was also supported by European Pankreas Zentrum (EPZ).

Data Availability Statement

The 16S rRNA sequencing data generated in this study are deposited in the NCBI BioProject database under accession number PRJNA1310990. Transcriptomic datasets analyzed in this study are publicly available from the NCBI GEO database (GSE15471, GSE56560, GSE62165, GSE62452, GSE71729). All other data supporting the findings of this study are available from the corresponding author upon reasonable request.

Author contributions

Y.Z., T.L.G., B. M., Z.H., H.S. and F.F. performed all the experiments. Pathology of animal tissues was undertaken by F.B. Clinical data were extracted by C.T., U.H., K. H., T.H., U. H. and F.F. 16S targeted

sequencing was performed by D.L. and microbiota analysis and statistical methods were undertaken by V.I., P.S., B.C. and F.F. General statistics were performed by U.H., M.S., B.M., R. K., B. B., M.S. and F.F.

The manuscript was written by Y.Z., V.I., and F.F. All reviewed the data, read the manuscript, and agreed with this version for submission. Y.Z., T.L.G., V. I. and F.F. undertook the design of the study.

Conflict of interest disclosure

The authors declare no competing interests.

References

1. Siegel RL, Wagle NS, Star J, Kratzer TB, Smith RA, Jemal A. Colorectal cancer statistics, 2026. CA Cancer J Clin. 2026;76(2):e70067.
2. Stoop TF, Javed AA, Oba A, Koerkamp BG, Seufferlein T, Wilmink JW, et al. Pancreatic cancer. Lancet. 2025;405(10485):1182-202.
3. Chen YE, Fischbach MA, Belkaid Y. Skin microbiota-host interactions. Nature. 2018;553(7689):427-36.
4. Westermann AJ, Gorski SA, Vogel J. Dual RNA-seq of pathogen and host. Nat Rev Microbiol. 2012;10(9):618-30.
5. Fang Y, Yang G, Yang J, Ren J, You L, Zhao Y. Human microbiota colonization and pancreatic ductal carcinoma. Crit Rev Microbiol. 2023;49(4):455-68.
6. Cossart P, Sansonetti PJ. Bacterial invasion: the paradigms of enteroinvasive pathogens. Science. 2004;304(5668):242-8.
7. Deretic V, Saitoh T, Akira S. Autophagy in infection, inflammation and immunity. Nat Rev Immunol. 2013;13(10):722-37.
8. Noda T, Yoshimori T. Molecular basis of canonical and bactericidal autophagy. Int Immunol. 2009;21(11):1199-204.
9. Hu W, Chan H, Lu L, Wong KT, Wong SH, Li MX, et al. Autophagy in intracellular bacterial infection. Semin Cell Dev Biol. 2020;101:41-50.
10. Thurston TL, Wandel MP, von Muhlinen N, Foeglein A, Randow F. Galectin 8 targets damaged vesicles for autophagy to defend cells against bacterial invasion. Nature. 2012;482(7385):414-8.
11. Wen X, Klionsky DJ. How bacteria can block xenophagy: an insight from Salmonella. Autophagy. 2020;16(2):193-4.
12. Greenfield LK, Jones NL. Modulation of autophagy by Helicobacter pylori and its role in gastric carcinogenesis. Trends Microbiol. 2013;21(11):602-12.
13. Pushalkar S, Hundeyin M, Daley D, Zambirinis CP, Kurz E, Mishra A, et al. The Pancreatic Cancer Microbiome Promotes Oncogenesis by Induction of Innate and Adaptive Immune Suppression. Cancer Discov. 2018;8(4):403-16.

14. Nejman D, Livyatan I, Fuks G, Gavert N, Zwang Y, Geller LT, et al. The human tumor microbiome is composed of tumor type-specific intracellular bacteria. Science. 2020;368(6494):973-80.
15. Fletcher AA, Kelly MS, Eckhoff AM, Allen PJ. Revisiting the intrinsic mycobiome in pancreatic cancer. Nature. 2023;620(7972):E1-E6.
16. Yin H, Pu N, Chen Q, Zhang J, Zhao G, Xu X, et al. Gut-derived lipopolysaccharide remodels tumoral microenvironment and synergizes with PD-L1 checkpoint blockade via TLR4/MyD88/AKT/NF-kappaB pathway in pancreatic cancer. Cell Death Dis. 2021;12(11):1033.
17. Riquelme E, Zhang Y, Zhang L, Montiel M, Zoltan M, Dong W, et al. Tumor Microbiome Diversity and Composition Influence Pancreatic Cancer Outcomes. Cell. 2019;178(4):795-806 e12.
18. Lee TS. Are Probiotics Beneficial or Harmful for Pancreatic Cancer Outcomes? Probiotics Antimicrob Proteins. 2024.
19. Diakopoulos KN, Lesina M, Wormann S, Song L, Aichler M, Schild L, et al. Impaired autophagy induces chronic atrophic pancreatitis in mice via sex- and nutrition-dependent processes. Gastroenterology. 2015;148(3):626-38 e17.
20. Xia L, Xu Z, Zhou X, Bergmann F, Grabe N, Buchler MW, et al. Impaired autophagy increases susceptibility to endotoxin-induced chronic pancreatitis. Cell Death Dis. 2020;11(10):889.
21. Antonucci L, Fagman JB, Kim JY, Todoric J, Gukovsky I, Mackey M, et al. Basal autophagy maintains pancreatic acinar cell homeostasis and protein synthesis and prevents ER stress. Proc Natl Acad Sci U S A. 2015;112(45):E6166-74.
22. Takamura A, Komatsu M, Hara T, Sakamoto A, Kishi C, Waguri S, et al. Autophagy-deficient mice develop multiple liver tumors. Genes Dev. 2011;25(8):795-800.
23. Ouimet M, Koster S, Sakowski E, Ramkhelawon B, van Solingen C, Oldebeken S, et al. Mycobacterium tuberculosis induces the miR-33 locus to reprogram autophagy and host lipid metabolism. Nat Immunol. 2016;17(6):677-86.
24. Fujii S, Mitsunaga S, Yamazaki M, Hasebe T, Ishii G, Kojima M, et al. Autophagy is activated in pancreatic cancer cells and correlates with poor patient outcome. Cancer Sci. 2008;99(9):1813-9.
25. Yang S, Wang X, Contino G, Liesa M, Sahin E, Ying H, et al. Pancreatic cancers require autophagy for tumor growth. Genes Dev. 2011;25(7):717-29.
26. Witte D, Pretzell I, Reissig TM, Stein A, Velthaus JL, Alig A, et al. Trametinib in combination with hydroxychloroquine or palbociclib in advanced metastatic pancreatic cancer: data from a retrospective, multicentric cohort (AIO AIO-TF/PAK-0123). J Cancer Res Clin Oncol. 2024;150(10):438.
27. McCubrey JA, Abrams SL, Follo MY, Manzoli L, Ratti S, Martelli AM, et al. Effects of chloroquine and hydroxychloroquine on the sensitivity of pancreatic cancer cells to targeted therapies. Adv Biol Regul. 2023;87:100917.
28. Fang YT, Yang WW, Niu YR, Sun YK. Recent advances in targeted therapy for pancreatic adenocarcinoma. World J Gastrointest Oncol. 2023;15(4):571-95.

29. Wolpin BM, Rubinson DA, Wang X, Chan JA, Cleary JM, Enzinger PC, et al. Phase II and pharmacodynamic study of autophagy inhibition using hydroxychloroquine in patients with metastatic pancreatic adenocarcinoma. Oncologist. 2014;19(6):637-8.
30. Karasic TB, O'Hara MH, Loaiza-Bonilla A, Reiss KA, Teitelbaum UR, Borazanci E, et al. Effect of Gemcitabine and nab-Paclitaxel With or Without Hydroxychloroquine on Patients With Advanced Pancreatic Cancer: A Phase 2 Randomized Clinical Trial. JAMA Oncol. 2019;5(7):993-8.
31. Zeh HJ, Bahary N, Boone BA, Singhi AD, Miller-Ocuin JL, Normolle DP, et al. A Randomized Phase II Preoperative Study of Autophagy Inhibition with High-Dose Hydroxychloroquine and Gemcitabine/Nab-Paclitaxel in Pancreatic Cancer Patients. Clin Cancer Res. 2020;26(13):3126-34.
32. Tanida I, Ueno T, Kominami E. LC3 and Autophagy. Methods Mol Biol. 2008;445:77-88.
33. Fortunato F, Burgers H, Bergmann F, Rieger P, Buchler MW, Kroemer G, et al. Impaired autolysosome formation correlates with Lamp-2 depletion: role of apoptosis, autophagy, and necrosis in pancreatitis. Gastroenterology. 2009;137(1):350-60, 60 e1-5.
34. Hingorani SR, Petricoin EF, Maitra A, Rajapakse V, King C, Jacobetz MA, et al. Preinvasive and invasive ductal pancreatic cancer and its early detection in the mouse. Cancer Cell. 2003;4(6):437-50.
35. Ariston Gabriel AN, Jiao Q, Yvette U, Yang X, Al-Ameri SA, Du L, et al. Differences between KC and KPC pancreatic ductal adenocarcinoma mice models, in terms of their modeling biology and their clinical relevance. Pancreatology. 2020;20(1):79-88.
36. Mizushima N, Yoshimori T. How to interpret LC3 immunoblotting. Autophagy. 2007;3(6):542-5.
37. Pust MM, Rocha Castellanos DM, Rzasa K, Dame A, Pishchany G, Assawasirisin C, et al. Absence of a pancreatic microbiome in intraductal papillary mucinous neoplasm. Gut. 2024;73(7):1131-41.
38. Moffitt RA, Marayati R, Flate EL, Volmar KE, Loeza SG, Hoadley KA, et al. Virtual microdissection identifies distinct tumor- and stroma-specific subtypes of pancreatic ductal adenocarcinoma. Nat Genet. 2015;47(10):1168-78.
39. Torre-Healy LA, Kawalerski RR, Oh K, Chrastecka L, Peng XL, Aguirre AJ, et al. Open-source curation of a pancreatic ductal adenocarcinoma gene expression analysis platform (pdacR) supports a two-subtype model. Commun Biol. 2023;6(1):163.
40. Huang Y, Zhu N, Zheng X, Liu Y, Lu H, Yin X, et al. Intratumor Microbiome Analysis Identifies Positive Association Between Megasphaera and Survival of Chinese Patients With Pancreatic Ductal Adenocarcinomas. Front Immunol. 2022;13:785422.
41. Zhong Y, Zhang D, Ding F, Zhang H, Guo Y, Huang Q, et al. Intratumoral microbiota-driven macrophage reprogramming in pancreatic cancer via Blautia metabolite 6-hydroxyhexanoic acid. Int Immunopharmacol. 2025;164:115421.
42. Zhou T, Wu J, Khan A, Hu T, Wang Y, Salama ES, et al. A probiotic Limosilactobacillus fermentum GR-3 mitigates colitis-associated tumorigenesis in mice via modulating gut microbiome. NPJ Sci Food. 2024;8(1):61.

43. Ye L, Hou Y, Hu W, Wang H, Yang R, Zhang Q, et al. Repressed Blautia-acetate immunological axis underlies breast cancer progression promoted by chronic stress. Nat Commun. 2023;14(1):6160.
44. Abe S, Masuda A, Matsumoto T, Inoue J, Toyama H, Sakai A, et al. Impact of intratumoral microbiome on tumor immunity and prognosis in human pancreatic ductal adenocarcinoma. J Gastroenterol. 2024;59(3):250-62.
45. Fang Y, Liu X, Ren J, Wang X, Zhou F, Huang S, et al. Integrated analysis of microbiome and metabolome reveals signatures in PDAC tumorigenesis and prognosis. Microbiol Spectr. 2024:e0096224.
46. Merali N, Chouari T, Sweeney C, Halle-Smith J, Jessel MD, Wang B, et al. The microbial composition of pancreatic ductal adenocarcinoma: a systematic review of 16S rRNA gene sequencing. Int J Surg. 2024;110(10):6771-99.
47. Gamboa-Tuz SD, Ramos M, Franzosa E, Huttenhower C, Segata N, Oh S, et al. Commonly used compositional data analysis implementations are not advantageous in microbial differential abundance analyses benchmarked against biological ground truth. bioRxiv 2025.
48. Kennedy KM, de Goffau MC, Perez-Munoz ME, Arrieta MC, Backhed F, Bork P, et al. Questioning the fetal microbiome illustrates pitfalls of low-biomass microbial studies. Nature. 2023;613(7945):639-49.
49. Li Y, Chang RB, Stone ML, Delman D, Markowitz K, Xue Y, et al. Multimodal immune phenotyping reveals microbial-T cell interactions that shape pancreatic cancer. Cell Rep Med. 2024;5(2):101397.
50. Tavano F, Napoli A, Gioffreda D, Palmieri O, Latiano T, Tardio M, et al. Could the Microbial Profiling of Normal Pancreatic Tissue from Healthy Organ Donors Contribute to Understanding the Intratumoral Microbiota Signature in Pancreatic Ductal Adenocarcinoma? Microorganisms. 2025;13(2).
51. Zhou X, An J, Kurilov R, Brors B, Hu K, Peccerella T, et al. Persister cell phenotypes contribute to poor patient outcomes after neoadjuvant chemotherapy in PDAC. Nat Cancer. 2023;4(9):1362-81.
52. Xu Z, Huang Z, Zhang Y, Sun H, Hinz U, Heger U, et al. Farnesoid X receptor activation inhibits pancreatic carcinogenesis. Biochim Biophys Acta Mol Basis Dis. 2023;1869(7):166811.
53. Mareninova OA, Sendler M, Malla SR, Yakubov I, French SW, Tokhtaeva E, et al. Lysosome associated membrane proteins maintain pancreatic acinar cell homeostasis: LAMP-2 deficient mice develop pancreatitis. Cell Mol Gastroenterol Hepatol. 2015;1(6):678-94.
54. Huang JY, Lee SM, Mazmanian SK. The human commensal Bacteroides fragilis binds intestinal mucin. Anaerobe. 2011;17(4):137-41.
55. Franks AH, Harmsen HJ, Raangs GC, Jansen GJ, Schut F, Welling GW. Variations of bacterial populations in human feces measured by fluorescent in situ hybridization with group-specific 16S rRNA-targeted oligonucleotide probes. Appl Environ Microbiol. 1998;64(9):3336-45.
56. Bustin SA. MIQE 2.0 and the Urgent Need to Rethink qPCR Standards. Int J Mol Sci. 2025;26(11).
57. Kartal E, Schmidt TSB, Molina-Montes E, Rodriguez-Perales S, Wirbel J, Maistrenko OM, et al. A faecal microbiota signature with high specificity for pancreatic cancer. Gut. 2022;71(7):1359-72.

58. Del Castillo E, Meier R, Chung M, Koestler DC, Chen T, Paster BJ, et al. The Microbiomes of Pancreatic and Duodenum Tissue Overlap and Are Highly Subject Specific but Differ between Pancreatic Cancer and Noncancer Subjects. Cancer Epidemiol Biomarkers Prev. 2019;28(2):370-83.
59. Martin FE, Nadkarni MA, Jacques NA, Hunter N. Quantitative microbiological study of human carious dentine by culture and real-time PCR: association of anaerobes with histopathological changes in chronic pulpitis. J Clin Microbiol. 2002;40(5):1698-704.
60. Kramski M, Gaeguta AJ, Lichtfuss GF, Rajasuriar R, Crowe SM, French MA, et al. Novel sensitive real-time PCR for quantification of bacterial 16S rRNA genes in plasma of HIV-infected patients as a marker for microbial translocation. J Clin Microbiol. 2011;49(10):3691-3.
61. Klindworth A, Pruesse E, Schweer T, Peplies J, Quast C, Horn M, et al. Evaluation of general 16S ribosomal RNA gene PCR primers for classical and next-generation sequencing-based diversity studies. Nucleic Acids Res. 2013;41(1):e1.
62. Caporaso JG, Lauber CL, Walters WA, Berg-Lyons D, Lozupone CA, Turnbaugh PJ, et al. Global patterns of 16S rRNA diversity at a depth of millions of sequences per sample. Proc Natl Acad Sci U S A. 2011;108 Suppl 1(Suppl 1):4516-22.
63. Nearing JT, Douglas GM, Hayes MG, MacDonald J, Desai DK, Allward N, et al. Author Correction: Microbiome differential abundance methods produce different results across 38 datasets. Nat Commun. 2022;13(1):777.
64. Nearing JT, Douglas GM, Hayes MG, MacDonald J, Desai DK, Allward N, et al. Microbiome differential abundance methods produce different results across 38 datasets. Nat Commun. 2022;13(1):342.
65. Zhou R, Ng SK, Sung JJY, Goh WWB, Wong SH. Data pre-processing for analyzing microbiome data - A mini review. Comput Struct Biotechnol J. 2023;21:4804-15.
66. Wirbel J, Essex M, Forslund SK, Zeller G. A realistic benchmark for differential abundance testing and confounder adjustment in human microbiome studies. Genome Biol. 2024;25(1):247.
67. Birebent R, Drubay D, Alves Costa Silva C, Marmorino F, Vitali G, Piccinno G, et al. Surrogate markers of intestinal dysfunction associated with survival in advanced cancers. Oncoimmunology. 2025;14(1):2484880.
68. Le Naour J, Montegut L, Pan Y, Scuderi SA, Cordier P, Joseph A, et al. Formyl peptide receptor-1 (FPR1) represses intestinal oncogenesis. Oncoimmunology. 2023;12(1):2237354.
69. Schettini F, Fontana A, Gattazzo F, Strina C, Milani M, Cappelletti MR, et al. Faecal microbiota composition is related to response to CDK4/6-inhibitors in metastatic breast cancer: A prospective cross-sectional exploratory study. Eur J Cancer. 2023;191:112948.
70. Idichi T, Seki N, Kurahara H, Yonemori K, Osako Y, Arai T, et al. Regulation of actin-binding protein ANLN by antitumor miR-217 inhibits cancer cell aggressiveness in pancreatic ductal adenocarcinoma. Oncotarget. 2017;8(32):53180-93.
71. Haider S, Wang J, Nagano A, Desai A, Arumugam P, Dumartin L, et al. A multi-gene signature predicts outcome in patients with pancreatic ductal adenocarcinoma. Genome Med. 2014;6(12):105.

72. Janky R, Binda MM, Allemeersch J, Van den Broeck A, Govaere O, Swinnen JV, et al. Prognostic relevance of molecular subtypes and master regulators in pancreatic ductal adenocarcinoma. BMC Cancer. 2016;16:632.
73. Yang S, He P, Wang J, Schetter A, Tang W, Funamizu N, et al. A Novel MIF Signaling Pathway Drives the Malignant Character of Pancreatic Cancer by Targeting NR3C2. Cancer Res. 2016;76(13):3838-50.

Tables

Tables are available in the Supplementary Files section.

Figures

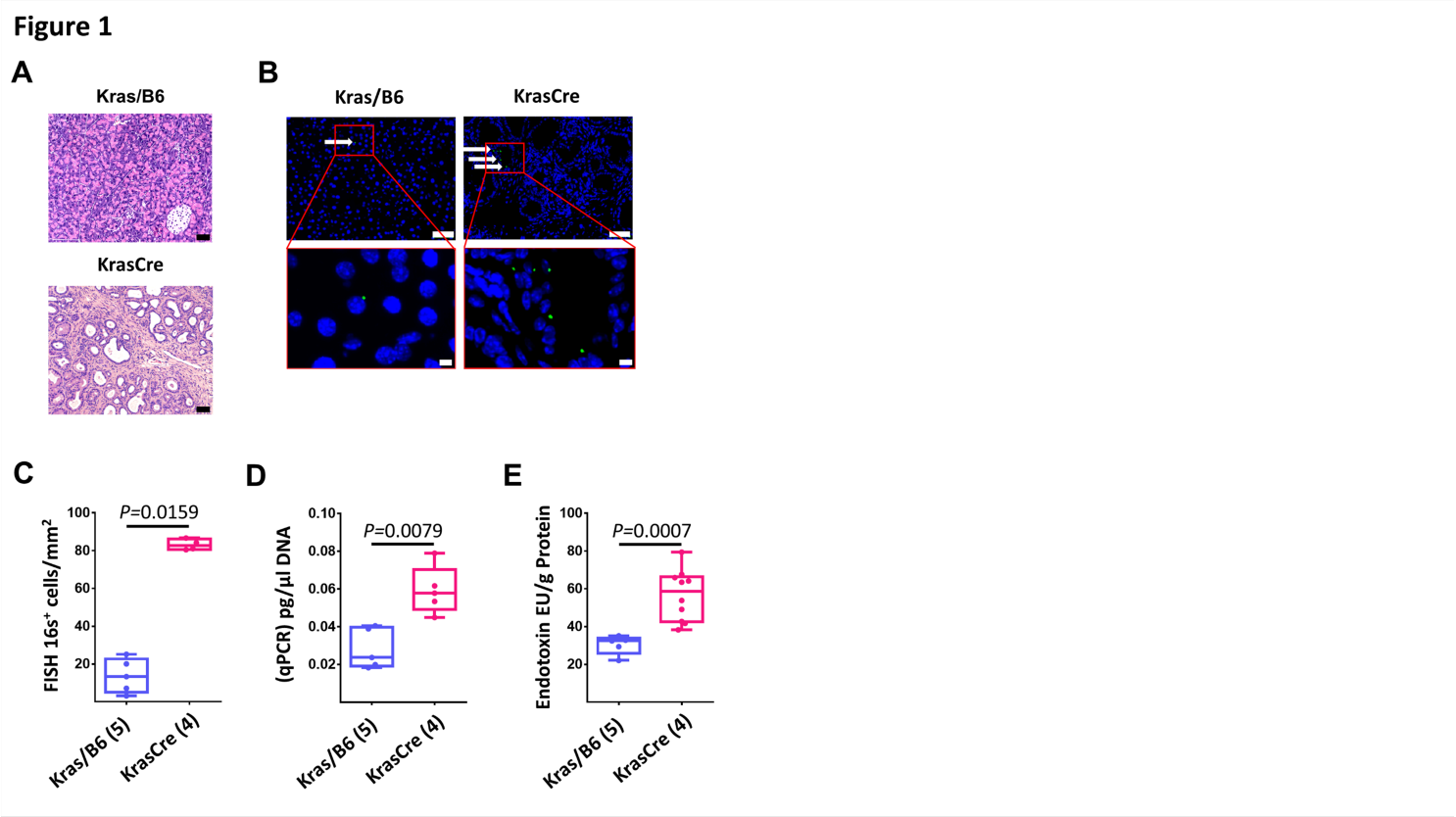


Figure 1

Increased bacterial colonization in mouse models of pancreatic Preneoplastic lesions. **(A)** Representative H&E stained pancreatic mouse tissue sections from KrasCre (PDAC precursor) mice and Kras/B6 control mice. Pancreatic disease exhibiting pancreatitis features with fibrosis, ADMs, PanIN lesions and pancreatic tumor precursor lesions. H&E staining images scalebar = 50 µm. **(B)** Representative fluorescence in situ hybridization (FISH) detecting bacterial 16S rRNA (green) in pancreatic tissue form KrasCre and Kras/B6 mice. Nuclei counterstaining with 4',6-diamidino-2-phenylindole (DAPI) (blue). Scalebar = 50 µm (overview) and 5 µm (magnified). **(C)** Box-and-whisker plots

with all points/animals shown. Quantitation of 16S rRNA FISH-positive cells per mm^2 pancreatic tissue in KrasCre and Kras/B6 mice. Differences between groups were assessed via the Mann-Whitney U test. Significance levels (*P*-values) are displayed above the respective bars/plots. **(D)** Box-and-whisker plots with all points/animals shown. Quantitation of pancreatic bacterial DNA by qPCR as relative 16S rRNA signals per µl of tissue DNA in KrasCre and Kras/B6 mice. Differences between groups were assessed via the Mann-Whitney U test. Significance levels (*P*-values) are displayed above the respective bars/plots. **(E)** Box-and-whisker plots with all points/animals shown. Endotoxin concentration in pancreatic extracts expressed as Endotoxin Units (EU) per g of extracted pancreatic protein from KrasCre and Kras/B6 mice. Differences between groups were assessed via the Mann-Whitney U test. Significance levels (*P*-values) are displayed above the respective bars/plots.

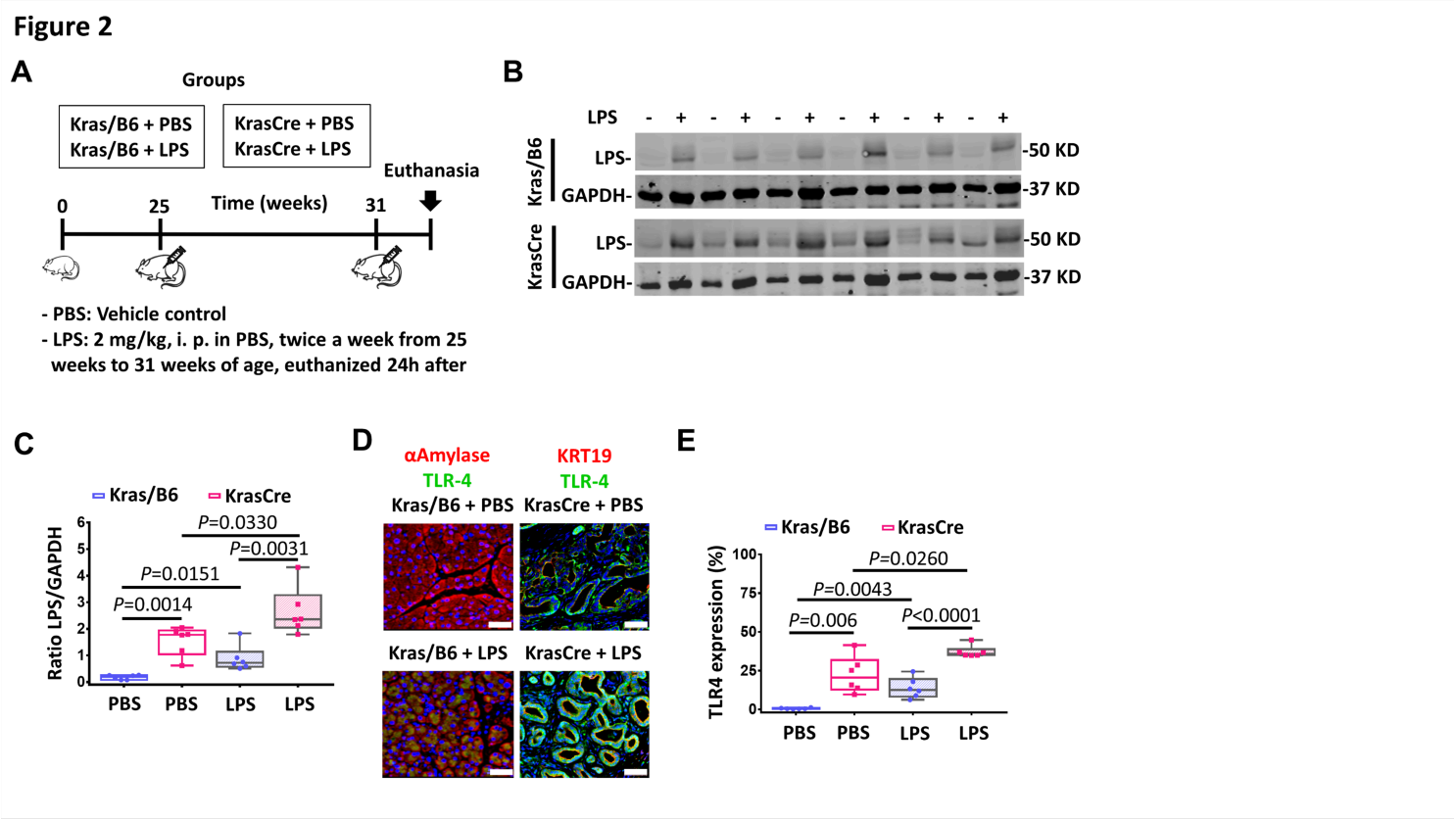


Figure 2

LPS enhance pancreatic TLR4 signaling and reduces Kreatin-19-positive neoplastic cells. (A) Schematic illustration of the experimental procedure for performing LPS injection (time-line). **(B)** Representative immunoblot images showing LPS and GAPDH (loading control) in KrasCre and Kras/B6 mice pancreata +/- LPS treatment. **(C)** Box-and-whisker plots with all points/animals shown. Densitometric quantification of LPS normalized to GAPDH (LPS/GAPDH ratio) in KrasCre and Kras/B6 mice with or without LPS treatment. Differences between groups were assessed via the Mann-Whitney U test. Significance levels (*P*-values) are displayed above the respective bars/plots. **(D)**Representative immunofluorescence (IF) images showing stained TLR4 co-stained with α-Amylase (Kras/B6 controls) or KRT19 (KrasCre). Scale bar, 50 µm. **(E)** Box-and-whisker plots with all points/animals shown.

Quantitation of TLR4 IF signal in KrasCre and Kras/B6 controls mice. Differences between groups were assessed via the Mann-Whitney U test. Significance levels (*P*-values) are displayed above the respective bars/plots.

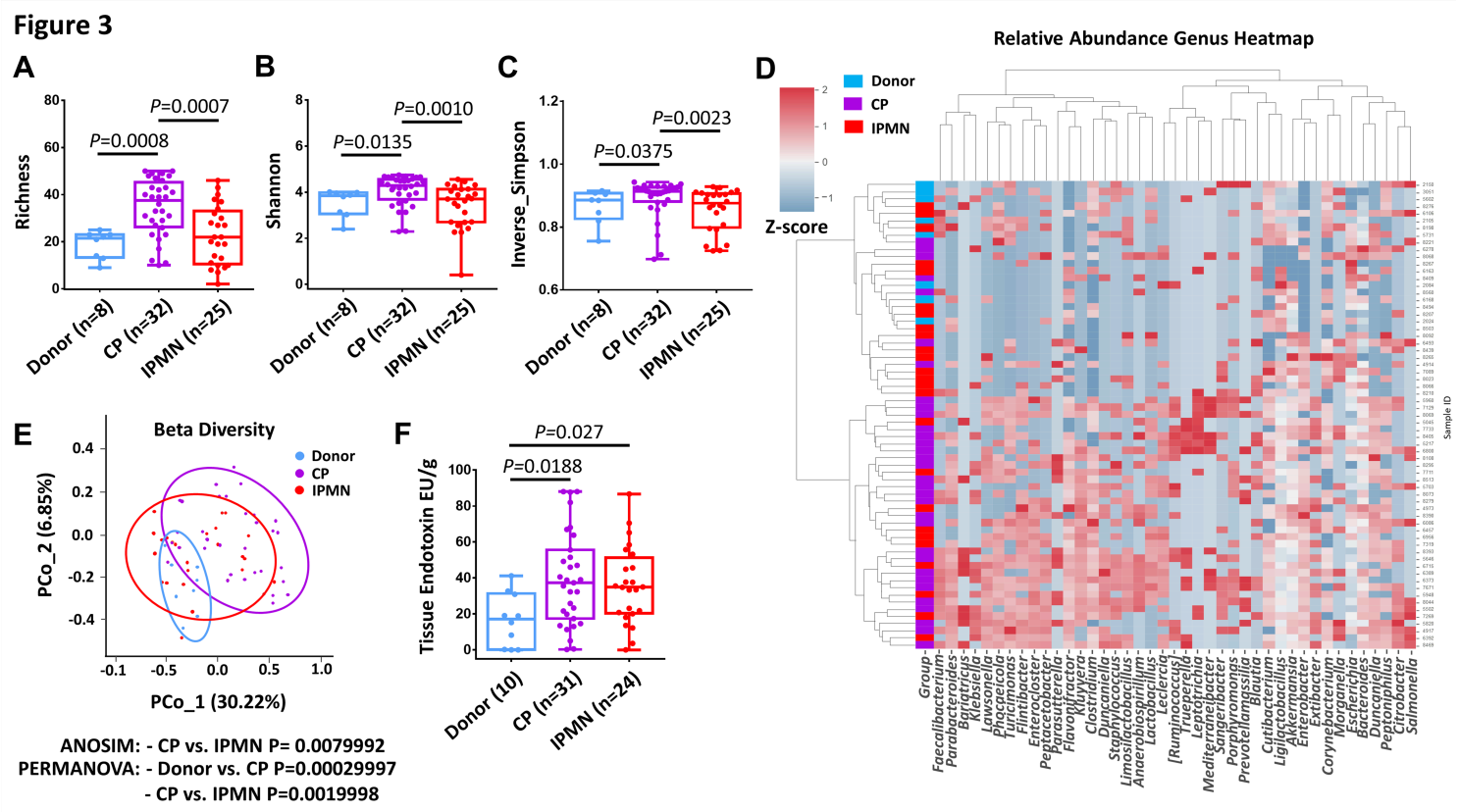


Figure 3

Distinct tissue microbiota profiles in chronic pancreatitis (CP) and intraductal papillary mucinous neoplasms (IPMN). (A) Box-and-whisker plots with all patients/points shown. Richness alfa-diversity index values in donor, CP and IPMN tissue. Differences between groups were assessed via the Mann-Whitney U test. Significance levels (*P*-values) are displayed above the respective bars/plots. **(B)** Box-and-whisker plots with all patients/points shown. Shannon alfa-diversity index values in donor, CP and IPMN tissue. Differences between groups were assessed via the Mann-Whitney U test. Significance levels (*P*-values) are displayed above the respective bars/plots. **(C)** Box-and-whisker plots with all patients/points shown. Inverse Simpson alfa-diversity index values in donor, CP and IPMN tissue. Differences between groups were assessed via the Mann-Whitney U test. Significance levels (*P*-values) are displayed above the respective bars/plots. **(D)** Heatmap/Clustermap of Z-scored relative abundances of microbial genera showing distinct community pattern with donor controls and IPMN co-clustering in cluster 1 and CP samples predominantly in cluster 2 (Freeman-Halton extension of Fisher´s exact test, two-tailed $P = 3.28*10^{-5}$). **(E)** Principal coordinate analysis (PCoA) of beta diversity showing between-group differences in community composition among CP, IPMN, and donor controls. Significance was assessed using ANOSIM and PERMANOVA (1000 permutations) and assessed using Kruskal-Wallis and pairwise Mann-Whitney tests with *P*-values. **(F)** Box-and-whisker plots with all patients/points shown. Endotoxin levels

measured by enzymatic assay in pancreatic tissue homogenate from donor controls, CP, and IPMN patients. Differences between groups were assessed via the Mann-Whitney U test. Significance levels (*P*-values) are displayed above the respective bars/plots.

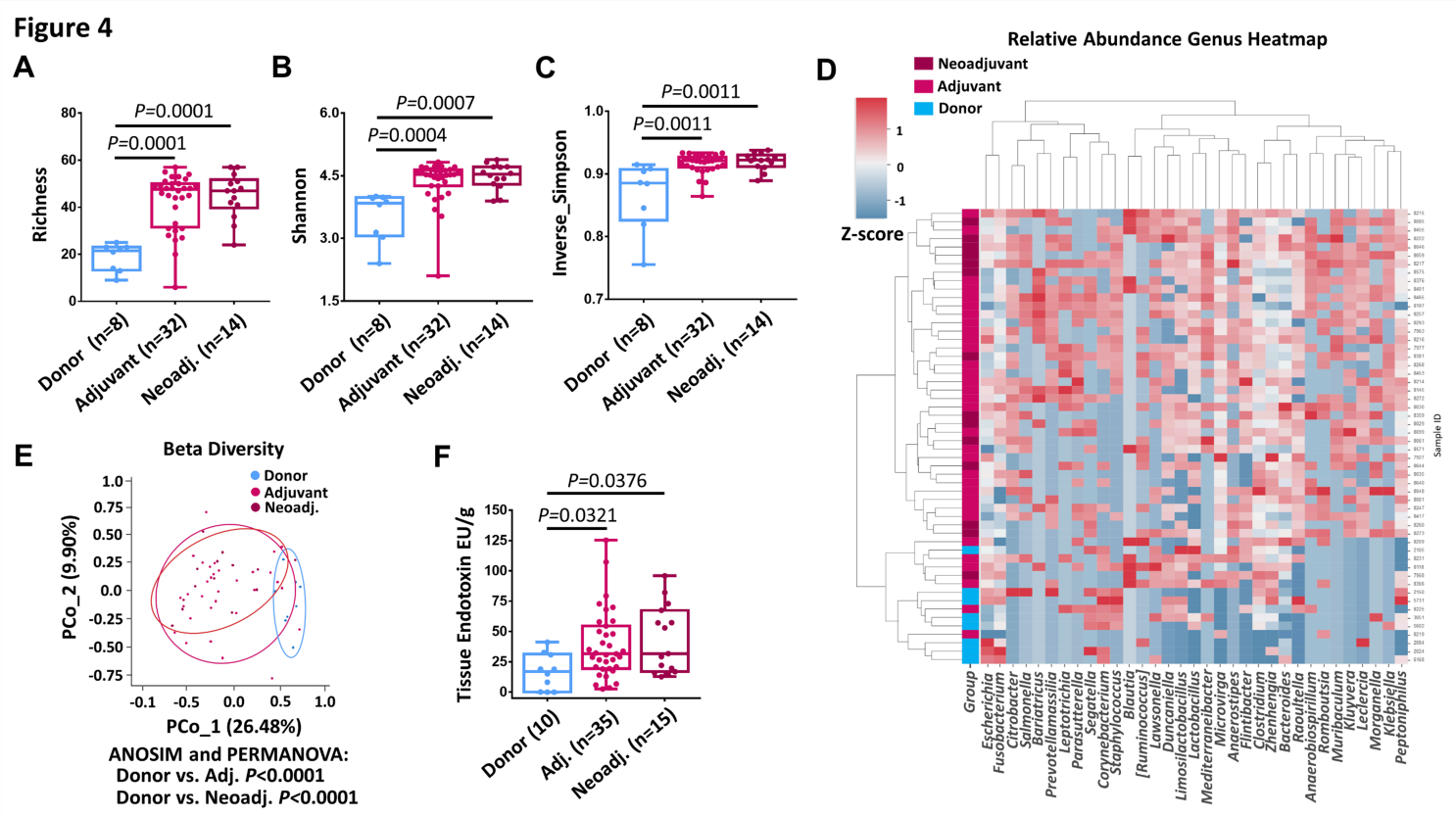


Figure 4

Distinct microbiota profiles in adjuvant (chemo-naive) and neoadjuvant pancreatic ductal adenocarcinoma (PDAC) patients. (A) Box-and-whisker plots with all patients/points shown. Richness alfa-diversity index values in donor controls, adjuvant (chemo-naive) and neoadjuvant PDAC tissue. Differences between groups were assessed via the Mann-Whitney U test. Significance levels (*P*-values) are displayed above the respective bars/plots. **(B)** Box-and-whisker plots with all patients/points shown. Shannon alfa-diversity index values in donor controls, adjuvant (chemo-naive) and neoadjuvant PDAC tissue. Differences between groups were assessed via the Mann-Whitney U test. Significance levels (*P* -values) are displayed above the respective bars/plots. **(C)** Box-and-whisker plots with all patients/points shown. Inverse Simpson alfa-diversity index values in donor controls, adjuvant (chemo-naive) and neoadjuvant PDAC tissue. Differences between groups were assessed via the Mann-Whitney U test. Significance levels (*P*-values) are displayed above the respective bars/plots. **(D)** Heatmap/Clustermap of Z-scored relative abundances of microbial genera showing co-clustering of adjuvant (chemo-naive) and neoadjuvant PDAC samples in cluster 1 (Freeman-Halton extension of Fisher´s exact test, two-tailed $P=1.04*10^{-5}$) **(E)** Principal coordinate analysis (PCoA) of beta diversity showing between-group differences in community composition among donor controls, adjuvant (chemo-naive) and neoadjuvant PDAC patients. Significance was assessed using ANOSIM and PERMANOVA (1000 permutations) and

assessed using Kruskal-Wallis and pairwise Mann-Whitney tests with *P*-values. **(F)** Box-and-whisker plots with all patients/points shown. Endotoxin levels measured by enzymatic assay in pancreatic tissue homogenate from donor controls, adjuvant (chemo-naive) and neoadjuvant PDAC patients. Differences between groups were assessed via the Mann-Whitney U test. Significance levels (*P*-values) are displayed above the respective bars/plots.

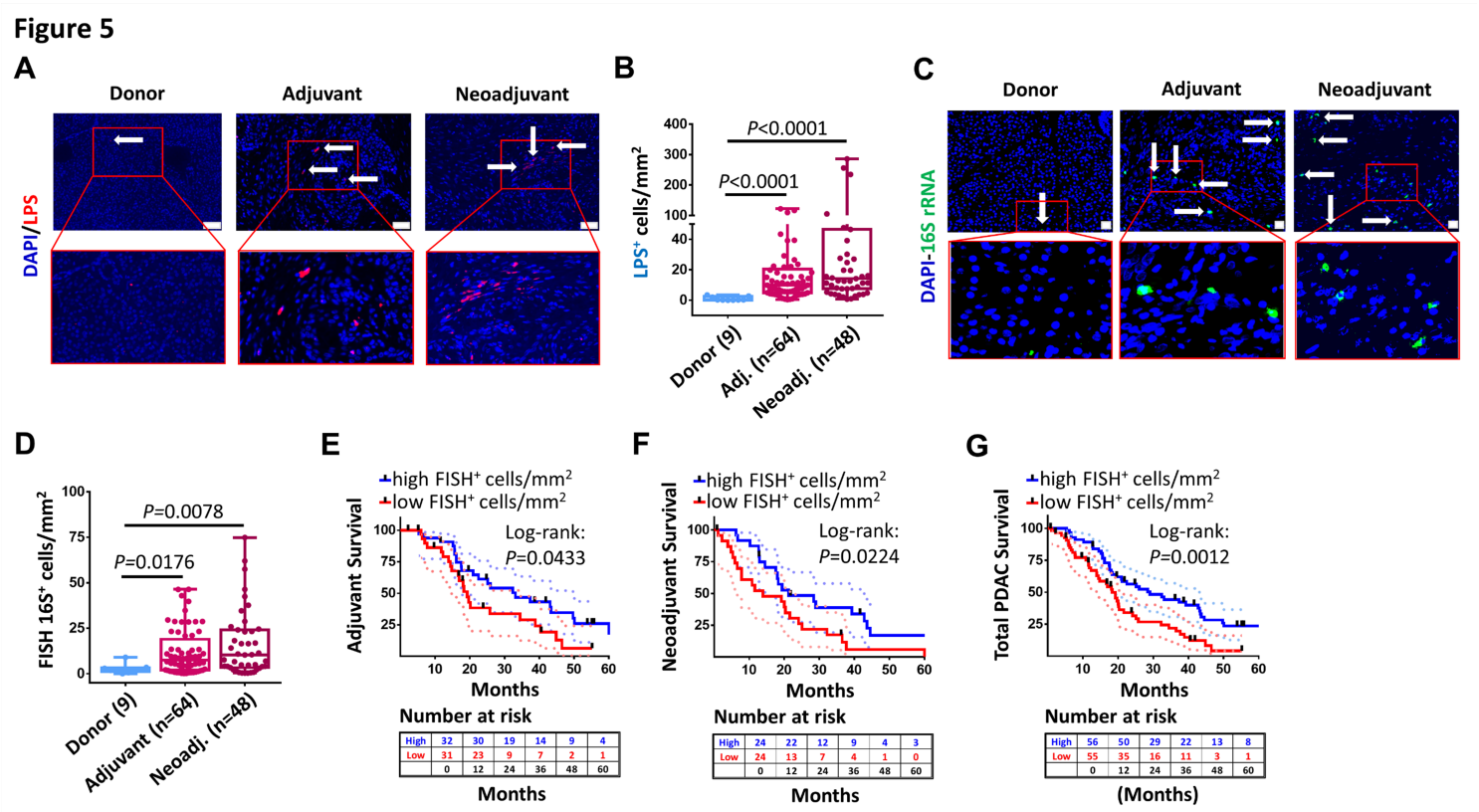


Figure 5

Increased bacterial LPS and elevated bacterial FISH signal are associate with improved survival for adjuvant and neoadjuvant pancreatic ductal adenocarcinoma (PDAC) patients. (A) Representative immunofluorescence images of pancreatic tissue from donor controls, adjuvant (chemo-naive) and neoadjuvant PDAC patients stained for LPS. Higher-magnification images highlight LPS-positive structures (scale bar = 50 µm). **(B)** Box-and-whisker plots with all patients/points shown. Quantitation of LPS-positive cells per mm^2 tissue from donor controls, adjuvant (chemo-naive) and neoadjuvant PDAC patients. Differences between groups were assessed via the Mann-Whitney U test. Significance levels (*P*-values) are displayed above the respective bars/plots. **(C)** Representative 16S rRNA FISH images in donor controls, adjuvant (chemo-naive), and neoadjuvant PDAC tissue with higher magnification. Arrows indicate 16S rRNA FISH-positive (Scale bar = 20 µm). **(D)** Box-and-whisker plots with all patients/points shown. Quantitation of 16S rRNA FISH-positive cells per mm^2 tissue in donor controls, adjuvant (chemo-naive), and neoadjuvant PDAC tissue. Differences between groups were assessed via the Mann-Whitney U test. Significance levels (*P*-values) are displayed above the respective bars/plots. **(E)** Kaplan-Meier survival analysis stratified by 16S rRNA FISH positive cells per mm^2 in adjuvant PDAC patients. Log-rank

test *P*-values and numbers at risk are shown. **(F)** Kaplan-Meier survival analysis stratified by 16S rRNA FISH positive cells per mm^2 in neoadjuvant (chemo-naive) PDAC patients. Log-rank test *P*-values and numbers at risk are shown. **(G)** Kaplan-Meier survival analysis stratified by 16S rRNA FISH positive cells per mm^2 in combined PDAC cohort. Log-rank test *P*-values and numbers at risk are shown.

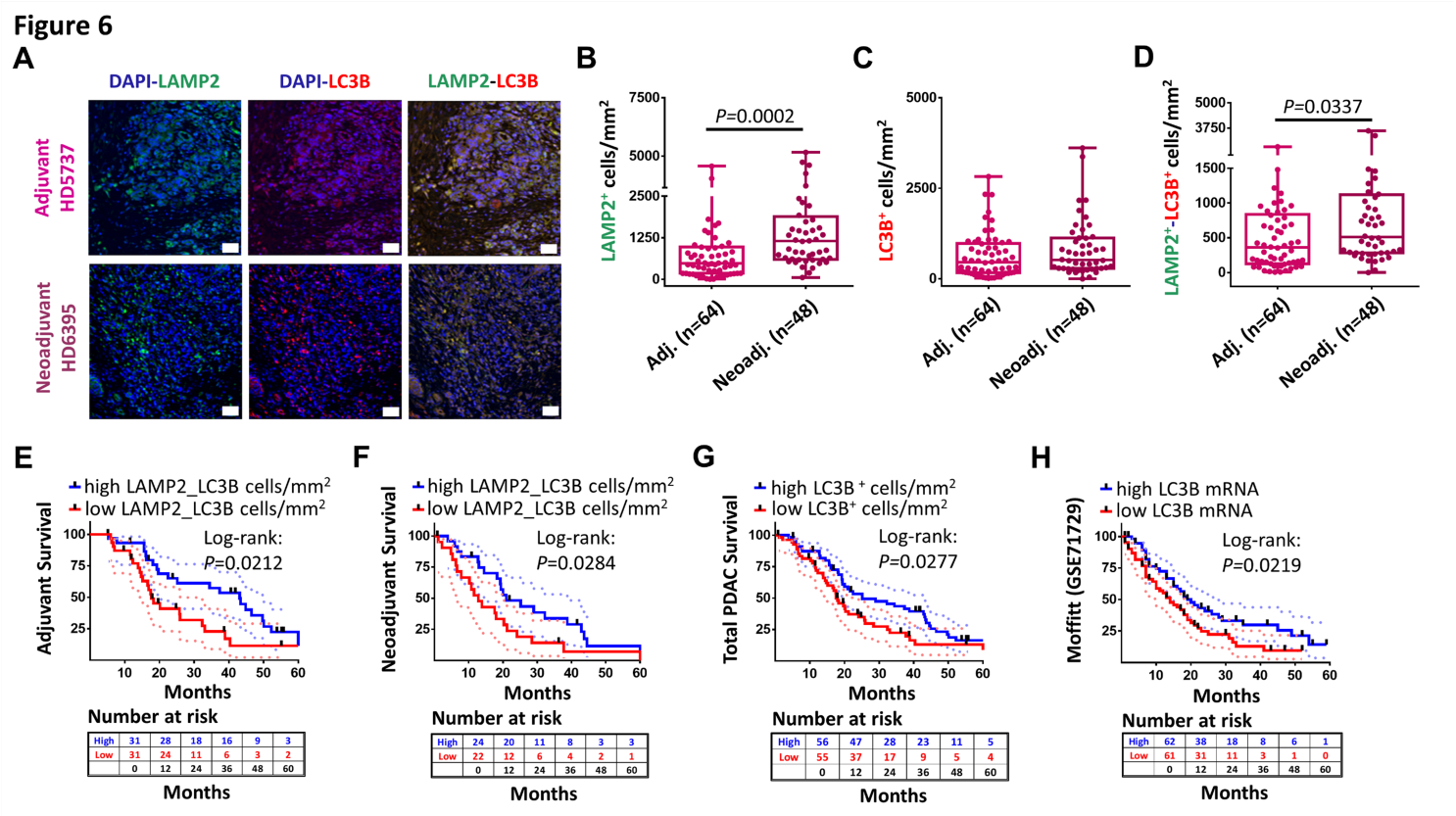


Figure 6

Increased autophagic markers LAMP2 and LC3B correlate with improved survival for adjuvant and neoadjuvant pancreatic ductal adenocarcinoma (PDAC) patients.

(A) Representative immunofluorescence images of pancreatic tissue from donor controls, adjuvant (chemo-naive) and neoadjuvant PDAC patients stained for LAMP2 and LC3B (scale bar = 50 µm). **(B)** Box-and-whisker plots with all patients/points shown. Quantitation of LAMP2-positive cells per mm^2 tissue in adjuvant (chemo-naive), and neoadjuvant PDAC tissue. Differences between groups were assessed via the Mann-Whitney U test. Significance levels (*P*-values) are displayed above the respective bars/plots. **(C)** Box-and-whisker plots with all patients/points shown. Quantitation of LC3B-positive cells per mm^2 tissue in adjuvant (chemo-naive), and neoadjuvant PDAC tissue. Differences between groups were assessed via the Mann-Whitney U test. Significance levels (*P*-values) are displayed above the respective bars/plots. **(D)** Box-and-whisker plots with all patients/points shown. Quantitation of LAMP2 and LC3B double-positive (autophagosome-positive) cells per mm^2 tissue in adjuvant (chemo-naive), and neoadjuvant PDAC tissue. Differences between groups were assessed via the Mann-Whitney U test. Significance levels (*P*-values) are displayed above the respective bars/plots. **(E)** Kaplan-Meier survival

analysis stratified by LAMP2_LC3B double-positive cells per mm^2 in adjuvant (chemo-naive) PDAC patients. Log-rank test *P*-values and numbers at risk are shown. **(F)** Kaplan-Meier survival analysis stratified by LAMP2_LC3B double-positive cells per mm^2 in neoadjuvant PDAC patients. Log-rank test *P*-values and numbers at risk are shown. **(G)** Kaplan-Meier survival analysis stratified by LC3B positive cells per mm^2 in combined adjuvant and neoadjuvant PDAC patients. Log-rank test *P*-values and numbers at risk are shown. **(H)** Kaplan-Meier survival analysis stratified by LC3B mRNA expression profile using the public available Moffitt cohort (GSE71729) in adjuvant PDAC patients (38). Log-rank test *P*-values and numbers at risk are shown.

Supplementary Files

This is a list of supplementary files associated with this preprint. Click to download.

- Supple.Figure3.tif
- Supple.Figure1.tif
- Table1C.xlsx
- Supple.Figure7.tif
- Supple.Figure2.tif
- Supple.Figure6.tif
- Supple.Table1.xlsx
- Table1A.xlsx
- Supple.Figure4.tif
- Table1B.xlsx
- Supple.Figure5.tif